Optics Letters

Constructing an achromatic polarization-dependent bifocal metalens with height-gradient metastructures

Xiang Xiong,[1] Xi Wang,[1] Zhenghan Wang,[1] Yajun Gao,[1] Ruwen Peng,[1,3] and Mu Wang[1,2,4]

[1]National Laboratory of Solid State Microstructures, School of Physics, and Collaborative Innovation Center of Advanced Microstructures, Nanjing University, Nanjing 210093, China
[2]American Physical Society, 1 Research Road, Ridge, New York 11961, USA
[3]e-mail: rwpeng@nju.edu.cn
[4]e-mail: muwang@nju.edu.cn

Received 12 November 2020; revised 7 January 2021; accepted 7 January 2021; posted 8 February 2021 (Doc. ID 414668); published 3 March 2021

Metalenses possess the extraordinary capability to tailor the wavefront of light with compact metastructures. However, it remains challenging to eliminate chromatic aberration and realize multifunctionality. Here we report an achromatic bifocal metalens (ABM) made of three-dimensional standing nano blocks (SNBs). By introducing a height gradient to SNBs, the ABM can achieve achromatic focusing in the wavelength range of 760–1550 nm with two different focal lengths by merely orthogonally switching the linear polarization of the incident beam. Such an achromatic multi-functional element may have applications in polarization sensing/display and shared-aperture optics design, among many others. © 2021 Optical Society of America

https://doi.org/10.1364/OL.414668

Lenses in optics change the wavefront of light, generating the effect of focusing or defocusing. For conventional lenses, the wavefront is shaped by the phase shift induced by the thickness of optical material [1]. This approach is usually bulky and heavy, so it becomes challenging for integrated optical systems. Recently developed metasurface lenses (metalenses) have shown clear privilege comparing with conventional lenses regarding size and weight [2–5]. Besides, a variety of exotic functionalities have been demonstrated with metalenses [6–11]. However, despite the developments, chromatic aberration and multifunctionality remain the issues for practical applications.

The chromatic aberration stands for the effect that occurs when a lens is unable to focus the light of different wavelengths to the same focal point. To solve this problem, hybridized glasses, such as achromatic doublets [12], have been developed to correct the chromatic aberration. Alternatively, diffractive optical elements can be used to compensate for the chromatic aberration of conventional optical materials [13]. These two approaches are unlikely to meet the critical requirements in weight and volume for integrated photonics. For metalenses constructed with periodically arranged units, the grating equation determines that the sine value of the diffraction angle of light is proportional to the wavelength [5]. Meanwhile, the electromagnetic (EM) response modes vary with the wavelength [14]. Therefore, many metalenses are applicable to a single wavelength or very narrow wavelength ranges.

Much effort has been devoted to eliminating the chromatic aberration of metalenses [5,15–17]. One approach combines multiple sub-metalenses with the same focal length, but working at different wavelengths into a metalens assembly [18–20]. By taking the advantage of the geometric phase modulation and multiple Fabry–Perot resonances, achromatic metalenses have been achieved [7,9,21]. By using multi-photon lithography, a hybrid achromatic metalens combining recursive ray-tracing and simulated phase libraries can offer improved focusing efficiency over a certain wavelength range [22]. A flat multilevel diffractive metalens composed of concentric rings of equal width but varying heights also shows achromatic imaging performance in the short-wave infrared band [23]. In previous studies, it is still difficult for the achromatic metalenses to provide multifunctionality.

The two-photon absorption (TPA) technique has provided more degrees of freedom to recent variable height metastructure designs [24–27]. In this Letter, we experimentally demonstrate an achromatic bifocal metalens (ABM) constructed with height-gradient metastructures. The ABM can reflect and converge the linearly polarized lights to the same position in a broadband wavelength range. The focal length of the ABM can be switched by rotating the polarized direction to the orthogonal direction. By arranging meta-atoms with different height gradients in orthogonal directions, bi-focusing is obtained with two different focusing spots. To the best of our knowledge, this is the first experimental demonstration of integrating broadband achromatic and switchable bi-focusing into one single metalens.

The schematic diagram of the achromatic metalens is shown in Fig. 1(a). The broadband incident light polarizing along the y direction is reflected and converged to the same focal position. Figure 1(b) shows the SNB meta-atom. The meta-atom is fabricated by TPA fabrication which is introduced in

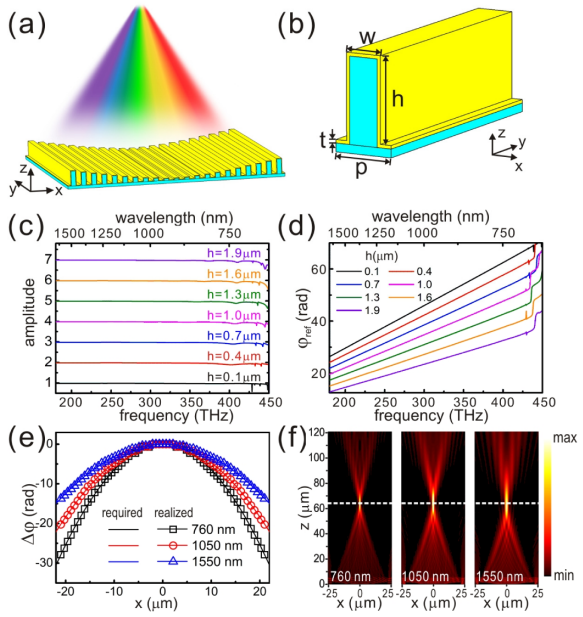

Fig. 1. (a) Schematic diagram of the achromatic metalens. (b) Detailed structure of the SNB meta-atom: $p = 0.7$ μm, $w = 0.35$ μm, and t is 40 nm. The calculated (c) amplitudes and (d) phase of the reflected light of different heights h are shown. Each curve in (c) is shifted by 1 from the previous curve along the y axis for clarity. (e) Theoretically required phase profile and the realized phase profile by using SNB meta-atoms. (f) Simulated intensity profiles in the $x - z$ planes.

Supplement 1. The height h of each SNB meta-atom is precisely adjusted, while all the other geometric parameters are identical. The bottom plane between the two standing blocks plays the role of a reference plane, and the height of the SNB decides the reflection phase of the EM waves. For normal incidence, no EM field is trapped between the neighboring standing blocks near the bottom.

To focus with the metalens, the required phase compensation of each meta-atom at the spatial position x should satisfy

$$\frac{\Delta\varphi(x, f)}{f} = \frac{\varphi(x, f) - \varphi(0, f)}{f} = \frac{2\pi}{c}[F - (x^2 + F^2)^{1/2}], \tag{1}$$

where f is the frequency of the incident light, F is the focal length of the metalens, and c is the light speed in vacuum [5]. According to Eq. (1), for an achromatic metalens, the phase compensation $\Delta\varphi(x, f)$ should meet the following two requirements. One is that for a certain spatial position x, $\Delta\varphi(x, f)$ should be linearly proportional to the frequency f; the other is that for different spatial position x, the ratio $\Delta\varphi(x, f)/f$ changes as the term of $[F - (x^2 + F^2)^{1/2}]$ changes. Once these two requirements are satisfied, the focal length F will keep invariant for different wavelengths [28,29].

The finite-difference time-domain method is applied in our simulation [30,31]. Figure 1(c) shows the simulated reflection amplitudes for the SNB meta-atoms of different heights. When h varies from 0.1 to 1.9 μm, the reflection amplitudes remain larger than 90% from 180 to 400 THz. In this frequency range, the uniformity of the amplitudes satisfies the generalized Snell law [2]. We choose the bottom plane between the standing blocks to define the reflection phase. As shown in Fig. 1(d), the reflection phases represent good linearity from 180 to 400 THz. Meanwhile, in this frequency range, the slop of φ_{ref} decreased gradually with the increment of the height h. The achromatic focusing mechanism is that we keep the phase shift provided by SNBs a constant at the focal point for different wavelengths. Meanwhile, the normal incident beams of different wavelengths focus at the same position and possess the same optical path.

In the simulation, a total of 61 SNB meta-atoms form a height-gradient SNB array, and the height-gradient profiles are provided in Supplement 1, Table S1. The designed focal length is 64 μm. Figure 1(e) shows the theoretically required phase profiles of three typical wavelengths in different positions. The realized phase profiles provided by the SNB array are consistent with the theoretically required profiles. Figure 1(f) shows the simulated light intensities in the $x - z$ planes. The light intensities indicate that the metalens can reflect and converge the incident lights to the same focal position.

We fabricate the height-gradient SNB array by a TPA fabrication process. The designed focal length is 64 μm, and the height-gradient profile of the SNB meta-atoms is based on the data shown in Supplement 1, Table S1. Figures 2(a) and 2(b) illustrate the top-view and the 45° tilted-angle view of the scanning electron micrograph (SEM) of the metalens. The size of the metalens in the $x - y$ plane is 42 μm × 42 μm, and the numerical aperture (NA) is 0.31. Figure 2(c) shows the measured light intensity distributions in the $x - y$ plane at $z = 64$ μm under the illuminations of different wavelengths. The illuminations are provided by light-emitting diodes. A wire grid polarizer is used, and the incident light polarizes along the y direction. Clear bright lines along the y direction can be observed at each wavelength. Additionally, in Fig. 2(d), we plot the intensity distributions of the reflected lights for different wavelengths in the $x - z$ plane. The metalens is mounted on a stage to adjust the distance between the metalens and the objective (Olympus, 10×). The measured full width at half-maximum (FWHM) values are shown in Supplement 1, Fig. S1. The focusing efficiency is shown in Fig. 2(e), which is defined as the fraction of the incident light that passes through a radius equal to three times the FWHM spot size [32]. The focusing efficiency is higher than 37% in the broadband wavelength range, and 48% focusing efficiency is obtained at 1450 nm. The relatively high focusing efficiency is mainly due to the uniform high reflection intensity and the linear phase profile provided by the SNB meta-atoms. The focal lengths vs incident wavelength are shown in Fig. 2(f). The error bars show the distance variations from the focal plane, where the intensity of the focal spot remains the maximum value in the measurements [7]. The reflected beams of various wavelengths are focused at nearly the same position. It should be mentioned that the fabrication error of the TPA process has diminished the focusing efficiency. Better achromatic focusing property and higher efficiency can be obtained by using more accurate 3D fabrication techniques.

The design approach of the ABM is to integrate two different SNB arrays working for the x- and y-polarized beams into one combined metalens. The x- and y-polarized incident lights can be reflected independently and converged to different focal positions. We fabricate the first SNB array working for y-polarized incident light first. The SNB meta-atoms are arranged along the x direction, and the designed focal length is 64 μm. Followed by that, we fabricate the second SNB array working for x-polarized incident light in the same area. The designed focal length of the

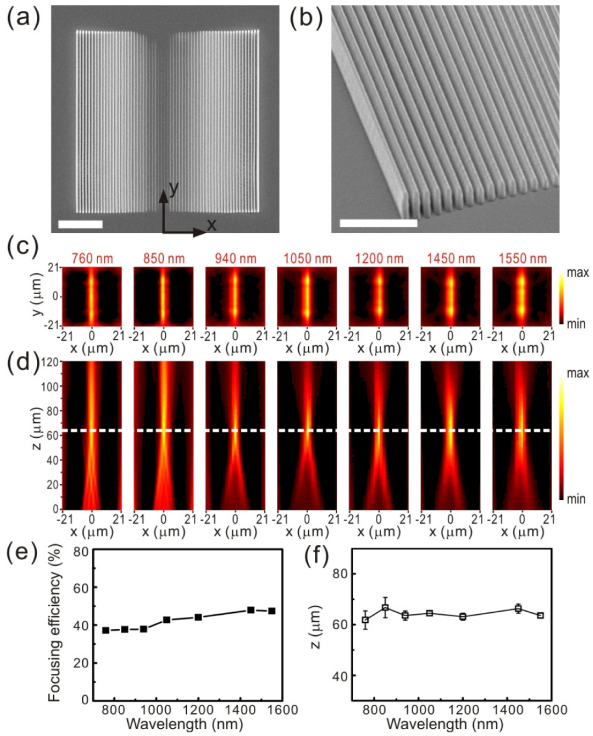

Fig. 2. (a) Top-view and (b) the 45° tilted-angle view SEM micrographs of the metalens. The scale bars represent 10 and 5 μm in (a) and (b), respectively. (c) Measured light intensity distributions at 64 μm above the metalens. (d) Measured intensity distributions of the reflected lights for different wavelengths in the $x-z$ plane. A charge-coupled device camera and an InGaAs camera are used to collect the intensity profiles. (e) Measured focusing efficiencies and (f) the measured focal lengths versus incident wavelengths.

second SNB array is 78 μm, and the NA is 0.26. The two height gradients of the ABM are shown in Supplement 1, Table S2.

The top-view and tilted-view SEM micrographs are shown in Figs. 3(a) and 3(b). We characterize the focusing property of the ABM. First, the y-polarized incident light illuminates the sample. Figure 3(c) shows the measured intensity distributions in the $x-y$ plane at $z=64$ μm. Clear bright lines along the y direction can be observed at different wavelengths. Figure 3(d) shows the intensity distributions of the reflected lights in the $x-z$ plane. The reflected beams of various wavelengths are focused at nearly the same position of $z=64$ μm. Then we rotate the polarizer by 90°, and the incident light is polarized in the x direction. Figures 3(e) and 3(f) demonstrate the measured intensity distributions in the $x-y$ and $y-z$ plane. This time the reflected beams of various wavelengths are focused at $z=78$ μm without chromatic aberration. The measured FWHM values for y- and x-polarized incident lights are shown in Supplement 1, Fig. S2. The measured focusing efficiencies for different polarizations are shown in Fig. 3(g). The focusing efficiencies are higher than 29% and 31% for y- and x-polarized incident lights, respectively. The focusing efficiency of the metalens is not affected by the integration of two SNB arrays in achieving bi-focusing functionality. When the polarization direction of the incidence is in the x or y direction, the gold surface of SNBs in the x or y direction will focus the light to one of the two focal positions. Since the reflection on the gold film does not change the polarization of light, two perpendicularly

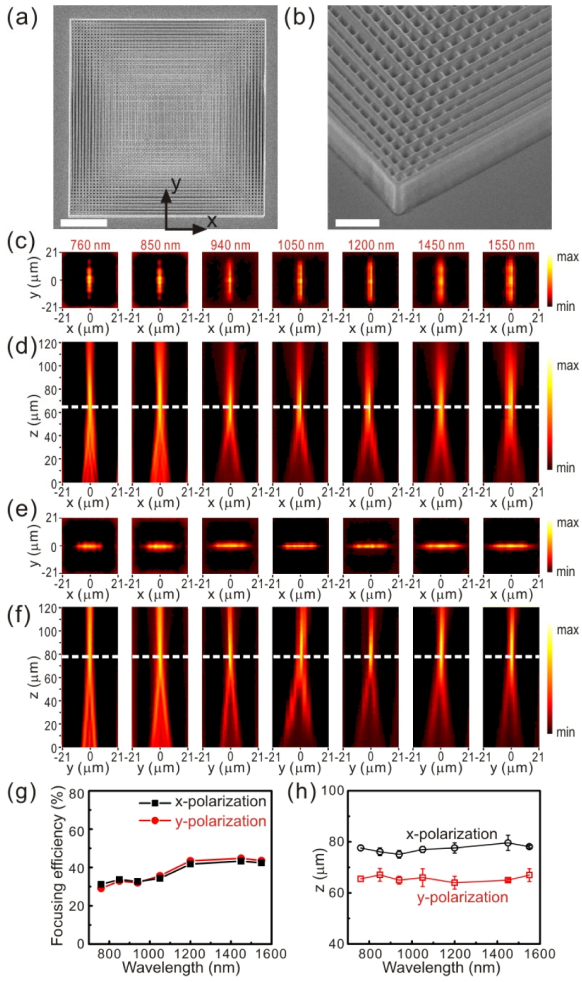

Fig. 3. (a) Top-view and (b) the 45° tilted-angle view SEM micrographs of the ABM. The scale bars represent 10 and 2 μm in (a) and (b), respectively. (c) Measured intensity distributions in the $x-y$ plane at 64 μm above the ABM and (d) the measured intensity distributions in the $x-z$ plane under y-polarized illuminations. (e) Measured intensity distributions in the $x-y$ plane at 78 μm above the ABM and (f) the measured intensity distributions in the $y-z$ plane under x-polarized illuminations. (g) Measured focusing efficiencies and (h) the focal lengths vs incident wavelength for x- and y-polarized incident lights.

polarized light will not interfere in focusing. Thus, the focusing efficiency of the metalens is not affected by the integration of two perpendicular SNB arrays in achieving bi-focusing functionality. The measured focal lengths vs incident wavelength for different polarizations are shown in Fig. 3(h). It is shown that by orthogonally rotating the polarization direction of the incident light, the focal length of the metalens can be switched between 64 and 78 μm in a broadband wavelength range.

In conventional variable focusing devices, mechanical moving elements are usually indispensable [33]. Such mechanical moving constructions in micro/nanoscale are costly, and their reliability is quite challenging. In our ABM design, there is no mechanical moving element. With high-speed polarization modulation techniques, such as the electro-optic polarization modulator, the speed of focal length modulation can be up to several tens of gigahertz [34]. On the other hand, the metalens made of SNBs has some limitations. In the fabrication process,

the SNBs higher than 2 μm can easily deform and adhere to each other. This will restrict the size of the metalens. For example, with the current material, the largest sizes of the metalens are 42 μm (NA = 0.31) and 70 μm (NA = 0.19), respectively. Besides, with our current design, the bandwidth of the ABM can be easily extended to 750–1700 nm. For a shorter wavelength, the reflection amplitudes drop below 90% due to EM absorption of the gold film. For a wavelength longer than 1700 nm, the 0 to 2π phase shift cannot be fulfilled with the required height gradient of SNBs because of the limitation of mechanical rigidity of the polymers.

In summary, we have experimentally demonstrated a broadband ABM based on height-gradient metastructures. The achromatic metalens can focus beams of different wavelengths to the same focal position without chromatic aberration. Meanwhile, the focal length can be switched by rotating the polarization direction of incident light to its perpendicular direction. We believe the height-gradient method may stimulate the optical integration technologies and expand the application scope of metastructures.

Funding. National Key Research and Development Program of China (2020YFA0211300, 2017YFA0303702); National Natural Science Foundation of China (11634005, 11674155, 11974177, 61975078).

Disclosures. The authors declare no conflicts of interest.

Supplemental document. See Supplement 1 for supporting content.

REFERENCES

1. E. Hecht, *Optics* (Pearson Education, 2017).
2. N. F. Yu, P. Genevet, M. A. Kats, F. Aieta, J. P. Tetienne, F. Capasso, and Z. Gaburro, Science **334**, 333 (2011).
3. M. Khorasaninejad, F. Aieta, P. Kanhaiya, M. A. Kats, P. Genevet, D. Rousso, and F. Capasso, Nano Lett. **15**, 5358 (2015).
4. E. Arbabi, A. Arbabi, S. M. Kamali, Y. Horie, M. Faraji-Dana, and A. Faraon, Nat. Commun. **9**, 812 (2018).
5. F. Aieta, M. A. Kats, P. Genevet, and F. Capasso, Science **347**, 1342 (2015).
6. M. Khorasaninejad and F. Capasso, Science **358**, eaam8100 (2017).
7. S. M. Wang, P. C. Wu, V. C. Su, Y. C. Lai, C. H. Chu, J. W. Chen, S. H. Lu, J. Chen, B. B. Xu, C. H. Kuan, T. Li, S. N. Zhu, and D. P. Tsai, Nat. Commun. **8**, 187 (2017).
8. X. Z. Chen, L. L. Huang, H. Muhlenbernd, G. X. Li, B. F. Bai, Q. F. Tan, G. F. Jin, C. W. Qiu, S. Zhang, and T. Zentgraf, Nat. Commun. **3**, 1198 (2012).
9. S. M. Wang, P. C. Wu, V. C. Su, Y. C. Lai, M. K. Chen, H. Y. Kuo, B. H. Chen, Y. H. Chen, T. T. Huang, J. H. Wang, R. M. Lin, C. H. Kuan, T. Li, Z. L. Wang, S. N. Zhu, and D. P. Tsai, Nat. Nanotechnol. **13**, 227 (2018).
10. X. Liu, J. Deng, K. F. Li, M. Jin, Y. Tang, X. Zhang, X. Cheng, H. Wang, L. Wei, and G. Li, Nanophotonics **9**, 3263 (2020).
11. S. Q. Li, S. H. Dong, S. X. Yi, W. K. Pan, Y. Z. Chen, F. X. Guan, H. J. Guo, Z. Wang, Q. He, and L. Zhou, Opt. Express **28**, 15601 (2020).
12. G. Beadie and J. N. Mait, Opt. Express **27**, 17771 (2019).
13. M. S. Millán, J. Otón, and E. Pérez-Cabré, Opt. Express **14**, 9103 (2006).
14. R. H. Fan, B. Xiong, R. W. Peng, and M. Wang, Adv. Mater. **32**, 1904646 (2020).
15. R. J. Lin, V.-C. Su, S. Wang, M. K. Chen, T. L. Chung, Y. H. Chen, H. Y. Kuo, J.-W. Chen, J. Chen, and Y.-T. Huang, Nat. Nanotechnol. **14**, 227 (2019).
16. A. Nemilentsau and T. Low, ACS Photonics **4**, 1646 (2017).
17. H. Zhou, L. Chen, F. Shen, K. Guo, and Z. Guo, Phys. Rev. Appl. **11**, 024066 (2019).
18. O. Avayu, E. Almeida, Y. Prior, and T. Ellenbogen, Nat. Commun. **8**, 14992 (2017).
19. J. T. Hu, C. H. Liu, X. C. Ren, L. J. Lauhon, and T. W. Odom, ACS Nano **10**, 10275 (2016).
20. E. Arbabi, A. Arbabi, S. M. Kamali, Y. Horie, and A. Faraon, Optica **3**, 628 (2016).
21. W. T. Chen, A. Y. Zhu, V. Sanjeev, M. Khorasaninejad, Z. J. Shi, E. Lee, and F. Capasso, Nat. Nanotechnol. **13**, 220 (2018).
22. F. Balli, M. Sultan, S. K. Lami, and J. T. Hastings, Nat. Commun. **11**, 3892 (2020).
23. S. Banerji, M. Meem, A. Majumder, C. Dvonch, B. Sensale-Rodriguez, and R. Menon, Opt. Continuum **2**, 2968 (2019).
24. S. J. Sun, Y. J. Gao, X. Xiong, R. W. Peng, and M. Wang, Opt. Lett. **44**, 1758 (2019).
25. Z. H. Wang, Y. S. Hu, X. Xiong, R. W. Peng, and M. Wang, Opt. Lett. **42**, 1153 (2017).
26. K. T. P. Lim, H. Liu, Y. Liu, and J. K. W. Yang, Nat. Commun. **10**, 25 (2019).
27. M. A. Sultan, F. Balli, D. L. Lau, and J. Hastings, "Hybrid metasurfaces for simultaneous focusing and filtering," arXiv:2009.07407 (2020).
28. S. Shrestha, A. C. Overvig, M. Lu, A. Stein, and N. Yu, Light: Sci. Appl. **7**, 85 (2018).
29. F. Presutti and F. Monticone, Optica **7**, 624 (2020).
30. Y.-J. Gao, X. Xiong, Z. Wang, F. Chen, R.-W. Peng, and M. Wang, Phys. Rev. X **10**, 031035 (2020).
31. X. Xiong, S. C. Jiang, Y. H. Hu, R. W. Peng, and M. Wang, Adv. Mater. **25**, 3994 (2013).
32. A. Arbabi, Y. Horie, A. J. Ball, M. Bagheri, and A. Faraon, Nat. Commun. **6**, 7069 (2015).
33. S.-H. Ahn and Y.-K. Kim, Sens. Actuators, A **78**, 48 (1999).
34. S. H. Wu, Y. Li, L. P. Feng, X. L. Zeng, W. Li, J. F. Qiu, Y. Zuo, X. B. Hong, H. Yu, R. Chen, I. P. Giles, and J. Wu, Opt. Lett. **43**, 2130 (2018).

210.28.142.243 (北京) 2021-07-06 03:00:43